XL CILAMCE
IBERO-LATIN AMERICAN CONGRESS ON COMPUTATIONAL METHODS IN ENGINEERING
NOVEMBER 11-14, 2019
Praiamar Natal Hotel & Convention Natal, RN-BRAZIL

YIELD DESIGN SOLUTIONS TO BEARING CAPACITY OF SHALLOW FOUNDATIONS RESTING ON THE SURFACE OF A GRANULAR SOIL REINFORCED BY A SOIL-CEMENT LAYER.

Aldo Fabián Yaharí Guillén
Aracely Belén Albariño Alfonso
Alejandro Quiñónez
Rubén Alcides López
María Alicia Arévalos
yahariguillen@gmail.com
a.belen96@gmail.com
rlopez@ing.una.py
rquinonez@ing.una.py
aliarevalos@gmail.com

Universidad Nacional de Asunción
Campus Universitario - San Lorenzo, 1760, Central, Paraguay

Abstract. Shallow foundations are recommended for suitable soils, in terms of bearing capacity and small settlements. For sites underlain loose soils, conventional practice is either to implement expensive deep foundations, or remove and replace the soft soils. In this context, soil improvement with admixtures (such as cement, lime, fly ash, slag, and combinations) turns to be a viable solution. However, designs procedures conceived to estimate bearing capacity improvement of such soils are based on empirical methodologies. The present work aims to study the ultimate bearing capacity problem of shallow foundations resting on the surface of a granular soil reinforced by a soil-cement layer. Such task is accomplished by means of the kinematic approach of the yield design theory through the implementation of several admissible virtual velocity fields, under plane strain conditions, for purely vertical loads. A parametric study is presented as a function of dimensionless parameters, which are defined from geometrical and strength properties. A comparison is then made, with available results obtained in the context of reduced models tests, under plane strain conditions. The maximum gap between the ultimate bearing capacity of the yield design theory and the reduced model tests was of about 18%.

Keywords: Bearing Capacity; Foundations; Limit Analysis, Yield Design.

INTRODUCTION

Shallow foundations are recommended for suitable soils, in terms of bearing capacity and small settlements. For sites underlain loose soils, conventional practice is either to implement expensive deep foundations, or remove and replace the soft soils. Several researches seek to find a methodology that allows the increase in soil bearing capacity for shallow foundations. Studies conducted in recent years show that it is possible to achieve such task by adding a soil-cement layer. [1]–[3]

The soil-cement is obtained from the mixture of soil, cement and water in adequate proportions, and has higher strength characteristics than natural soil. It has been used for decades in the area of pavement stabilization, as have other cementing products such as cement, lime, fly ash, slag, and combinations. [4]

An estimate of the increase of the ultimate bearing capacity of shallow foundations resting on the surface of a granular soil reinforced by a soil-cement layer can be made using the application of the yield design theory, which consists of two fundamental approaches: static approach, which allows to obtain loads for which the system will be stable and will not produce failure, and the kinematic approach, which defines the loads for which the system is ensured that the system fails. By maximizing and minimizing the obtained equations, the theoretical exact solution of the maximum permissible system load may be found.

STATEMENT OF THE PROBLEM

The present work relates to the ultimate bearing capacity of shallow foundations resting on the surface of a granular soil reinforced by a soil-cement layer. The foundation (width B) and the soil-cement layer (width B_r and depth H_r) are assumed to have an infinite length following *z* axis (plane strain situation). Loads are considered uniformly distributed on the *z* axis. The foundation is assumed rigid. Two mechanisms of failure are studied: Prandtl's mechanism and Hill's mechanism, for the case resting on the surface of soil-cement layer and the case of resting on natural soil.

The soil studied is granular, and therefore it is able to be modeled as Mohr-Coulomb material with friction angle ϕ and cohesion intercept C is null. The friction angle varies between values from $0°$ to $40°$. The gravity forces are taken into account in the analysis. The parameters on which the problem depends are: the vertical component of the load V, the internal friction angle ϕ and the density of the soil γ, as well as the geometry of the mechanism studied: the width B of the foundation; and the thickness H_r, over width T_r and width B_r of the soil-cement layer.

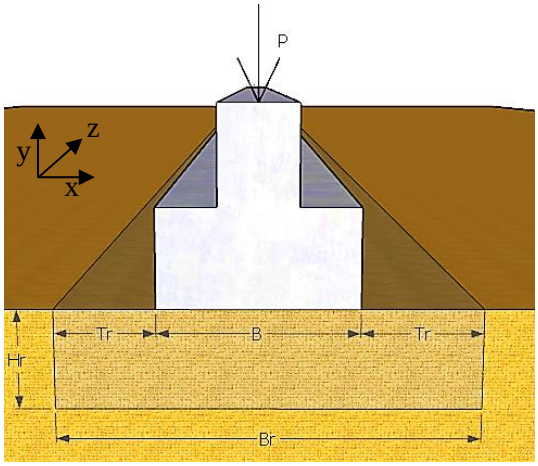

Figure 1. Shallow foundations resting on the surface of a granular soil reinforced by a soil-cement layer

The non-dimensional load capacity factor is defined as:

$$N_\gamma = \frac{2P}{\gamma B^2} \tag{1}$$

where P is the vertical load uniformly distributed per meter. Parameters m and n are used to relate the thickness H_r, over width T_r and width B_r of soil-cement layer to the width B of the footing:

$$H_r = nB \tag{2}$$

$$T_r = mH_r \tag{3}$$

$$B_r = (1+2mn)B \tag{4}$$

SOIL-CEMENT LAYER

The soil cement is a compacted mixture of soil, water and cement in a certain dosage, this material has an increased resistance to compression than natural soil and a very low permeability. All soils are suitable to be used as soil cement, however, the consumption of cement in the mixture and the workability of the material establish the limits of which type of soil to use. Those where the percentage of cement is between 5% and 12% of the weight of the material are considered suitable. Better results are obtained with sandy soils, soils with gravel, sandy soils with deficiency of fine particles, loamy soils and clay soils with low plasticity.[5]

Both soil-cement and cement paste are composed of sand (in the case of a granular soil), water and cement, their main difference being that the moisture content soil-cement are insufficient to cover the entire surface of the aggregates and fill the voids existing in the volume of the same.

Vendruscolo (1996) mentions that there are two types of reactions that appear due to soil-cement interaction: primary and secondary reactions. Primary reactions are those governing granular soils, while cohesive soils are more affected by secondary reactions. [6]

The same autor, quoting Moh (1956), represents this reactions as:

Primary reactions:

$Cement + H_2O \rightarrow CSH + Ca(OH)_2$ (Hydration)

$Ca(OH)_2 \rightarrow Ca^{++} + 2(OH)^-$ (Hydrolysis)

Secondary reactions:

$Ca^{++} + 2(OH)^- + SiO_2 \rightarrow CSH$

$Ca^{++} + 2(OH)^- + Al_2O_3 \rightarrow CAH$

Where: C = CaO, S = SiO_2, F = Fe_2O_3 and H = H_2O.

Foppa (2016) tested reduced models of surface foundations on a layer of soil-cement reinforcement. It was able to determine two characteristic types of failure. In the first case the foundation and the reinforcement behave as a single element that settles uniformly, the layer of reinforcement sinks into the natural soil without presenting cracks until the displacement corresponding to the load capacity of the natural soil, the rupture occurs in the base soil. In the second case the rupture occurs in the reinforcement layer due to the appearance of a fissure that is originated by the existence of an initial settlement, when the settlements increase the fissures propagate from bottom to top being able to be near the edge or in the axis of the foundation. [7]

The behavior of cemented soils is influenced by the density, the percentage of humidity and to a considerable measure by the degree of foundation that is also associated with the cohesion of the material. Recent tests conclude that the simple compression test for high densities the resistance is influenced by the density of the test bodies, increasing with it, while for low densities the resistance maintains constant values, independently of the density value [8]. On the other hand, in the cementing process, the granulometric distribution also has an incidence in the resistance, obtaining better results in fine soils and with a good granulometric distribution. [9]

In the case of reduced models tests of shallow foundations resting on soil-cement reinforced soils, the results indicate that the resistance of the soil-cement has no influence on the load capacity if

the failure is caused by punching, but it is an important value to know under which deformation values the reinforcement rupture occurs. [7]

Inglés and Metcalf (1972) provide an indicative table (Table 1) of the percentage of cement needed depending on soils with different characteristics.

Table 1. Cement quantity forecast depending on the type of soil. [10]

Soil Type	Cement Requirement (per cent)
Fine crushed rock	0,5 - 2
Well graded Sandy clay gravels	2 - 4
Well graded sand	2 - 4
Poorly graded sand	4 - 6
Sandy clay	4 - 6
Silty clay	6 - 8
Heavy clay	8 - 12
Very heavy clay	12 - 15
Organic soils	10 - 15

YIELD DESIGN THEORY

The problem presented was studied through the use of the cinematic approach of limit analysis theory. Due to the practical difficulties presented in the rigorous study of the static approach of the yield design theory, some analysis was also made through the use of the limit equilibrium method.

The limit equilibrium method is based on the construction of fault surfaces from various simple shapes such as planes, circular surfaces and logarithmic surfaces. This method was used by Terzaghi to determine the capacity of foundations, it is not accurate, but approximate results can still be obtained.

FUNDAMENTAL PRINCIPLES OF LIMIT ANALYSIS

Given a system of loads represented by $\underline{Q}_1$, $\underline{Q}_2$,..., $\underline{Q}_n$ acting on a three-dimensional continuous solid, volume Ω and contour $d\Omega$, for each point $\underline{x}$ of solid there is a strees state $\underline{\underline{\sigma}}$. It can be define strength domain $G(\underline{x})$ as the one where for all the points $\underline{x}$, strees state $\underline{\underline{\sigma}}$, strees are admissible.

This domain $G(\underline{x})$ has the property of being convex, zero is included and has a flow rule associated.

of loads $\underline{Q}_1$, $\underline{Q}_2$,..., $\underline{Q}_n$ by $\underline{Q}$, for a load to be statically admissible it must be fulfilled that:

$$\underline{Q} \text{ is admissible} \leftrightarrow \begin{cases} \exists \underline{\underline{\sigma}} \text{ S. A. on } \underline{Q}(\underline{x}) \wedge \underline{\underline{\sigma}}(\underline{x}) \in G(\underline{x}) \forall x \in \Omega \end{cases} \tag{5}$$

The set of permissible loads is denoted by K :

$$Q / \exists \underline{\underline{\sigma}} \text{ S. A. e } f(\underline{\underline{\sigma}}) \leq 0 \forall \underline{x} \in \Omega \tag{6}$$

If $\underline{Q}$ is located outside of K the system is unstable. A load $\underline{Q}^*$ is said to be a limit load if it is within the K contour called ∂K .[11]

1.1 STATIC APPROACH

Chen (1975) established the lower boundary theorem as follows: "The loads, determined for a distribution of tensions, which satisfy: a) the equations of equilibrium, b) the boundary stress conditions; and c) which nowhere violate the yield criterion, are not greater than the actual collapse

load". A statically admissible stress field is one that meets these conditions, here it is stated that if such a stress field can be found the fault will not occur for a lower load.[12]

From this premise all the load sets that comply with the hypotheses will be inside the K domain, so it is possible to find ∂K approaching inside the contour maximizing the $\underline{Q}$ values.

1.2 KINEMATIC APPROACH

This theorem is established as follows: "The loads, determined by equating the external working rate and the internal dissipation rate in a supposed deformation mode (velocity field) that satisfies: a) the limit conditions of velocity and, b) the conditions of compatibility of tension and velocity, are not lower than the actual collapse load". The kinematically permissible velocity field is the velocity field that complies with the above conditions. From this theorem it is possible to say that finding the velocity field that complies with the theorem, the acting load will indefectibly produce the failure of the system.[12]

In order to apply the theorem, it is necessary to assume the failure mechanism of the system, in a way that it fulfills the conditions. If the exact failure mechanism is found, the solution found will also be exact.

Similar to the case of the lower limit theorem, the upper limit theorem can also be used to find the ∂K contour but approaching from the outside since all the load values obtained through this theorem will be outside K, so ∂K can approximate minimizing the $\underline{Q}$ values.

An imposed load will not be permissible for a considered breaking mechanism if the load produces a rate of change in external energy or power greater than the internal rate of dissipation or deformation power. From this it can be said that the maximum power that can resist a mechanism considered is equal to the maximum value of the deformation power, this power receives the name of maximum resistant power, then:

$$P_{ex} \leq P_{rm} \tag{7}$$

The external power is defined as $P_{ex} = \underline{Q}(\underline{\underline{\sigma}}) \cdot \underline{\dot{q}}(\underline{U})$ where $\underline{U}$ is defined as a field of virtual velocities and $\underline{\dot{q}}$ the virtual velocities associated with the point of application of external loads.[11]

The maximum resistive power is set as:

$$P_{rm}(\underline{U}) = \int_{\Omega} \underline{\underline{\sigma}} : \underline{\underline{\hat{d}}} d\Omega + \int_{\Sigma_{\hat{U}}} (\underline{\underline{\sigma}}.[[\hat{\underline{U}}]]).\underline{n} d\Sigma \tag{8}$$

Where $\underline{\underline{\hat{d}}}$ denotes the rate of virtual deformations to the virtual velocity field $\underline{U}$, Σ denotes the surface of the mechanism where the velocity discontinuity occurs and $\underline{n}$ denotes a vector normal to the surface Σ.

Then it's possible to write that:

$$\underline{Q}(\underline{\underline{\sigma}}) \cdot \underline{\dot{q}}(\underline{U}) - P_{rm}(\underline{U}) \leq 0 \tag{9}$$

For this equation to provide valid results it must be fulfilled that:

$$\underline{\dot{q}}(\underline{U}) \neq 0 \wedge \mathrm{P}_{rm}(\underline{U}) < +\infty \tag{10}$$

1.3 THE PI FUNCTIONS

The π support functions are functions of the resistance domain that represent the maximum value that can be mobilized by the deformation power, they are auxiliary functions that allow to obtain the maximum resistant power for a certain mechanism.

The support functions depend on the $\underline{x}$ point of the solid and the local value of the deformation rate $\underline{\underline{d}}$. These functions are defined for different failure criterion, which in turn are selected according to the type of constituent material of the system to be analyzed.[11]

Generally speaking:

$$\int_\Omega \underline{\underline{\sigma}} : \hat{\underline{\underline{d}}} d\Omega = \int_\Omega \pi(\hat{\underline{\underline{d}}}) d\Omega \tag{11}$$

$$\int_{\Sigma_{\hat{\underline{U}}}} (\underline{\underline{\sigma}}.[[\hat{\underline{U}}]]).\underline{n} d\Sigma = \int_{\Sigma_{\hat{\underline{U}}}} \pi(\underline{n}, [[\hat{\underline{U}}]]) d\Sigma \tag{12}$$

This is finally equivalent to:

$$P_{rm}(\underline{U}) = \int_\Omega \pi(\hat{\underline{\underline{d}}}) d\Omega + \int_{\Sigma_{\hat{\underline{U}}}} \pi(\underline{n}, [[\hat{\underline{U}}]]) d\Sigma \tag{13}$$

1.4 CONSTITUENT MATERIALS

3.4.1 Mohr-Coulomb material

Resistance criterion:

$$f(\underline{\underline{\sigma}}) = \sup\left\{\sigma_i(1+\sin\phi) - \sigma_j(1-\sin\phi) - 2C\cos\phi \mid i,\ j = 1,2,3\right\} \tag{14}$$

Support function:

$$\pi(\hat{\underline{\underline{d}}}) = \frac{C}{\tan\phi} tr\hat{\underline{\underline{d}}} \ \textbf{if} \ tr\hat{\underline{\underline{d}}} \geq (\left|\hat{d}_1\right| + \left|\hat{d}_2\right| + \left|\hat{d}_3\right|)\sin\phi \tag{15}$$

$$\pi(\underline{n}, \left[\!\left[\hat{\underline{U}}\right]\!\right]) = \frac{C}{\tan\phi} \left[\!\left[\hat{\underline{U}}\right]\!\right].\underline{n} \ \textbf{if} \ \left[\!\left[\hat{\underline{U}}\right]\!\right].\underline{n} \geq \left|\left[\!\left[\hat{\underline{U}}\right]\!\right]\right| \sin\phi \tag{16}$$

C is the cohesion of the material and ϕ is the angle of internal friction which are the resistance parameters of the material.

The values of $i,\ j = 1,2,3$ represent the main stresses.

The Mohr-Coulomb Criteria is originally developed for the study of soils although it is also used to model the resistance of rocks and concrete. Principally, this method gives better results in the case of sandy soils.

3.4.2 Tresca material

Resistance criterion:

$$f(\underline{\underline{\sigma}}) = \sup\left\{\sigma_i - \sigma_j - \sigma_0 \mid i,\ j = 1,2,3\right\} \tag{17}$$

Support function:

$$\pi(\hat{\underline{\underline{d}}}) = \frac{\sigma_0}{2}(\left|\hat{d}_1\right| + \left|\hat{d}_2\right| + \left|\hat{d}_3\right|) \ \textbf{if} \ tr\hat{\underline{\underline{d}}} = 0 \tag{18}$$

$$\pi(\underline{n}, \left[\!\left[\hat{\underline{U}}\right]\!\right]) = \frac{\sigma_0}{2}\left\|\left[\!\left[\hat{\underline{U}}\right]\!\right]\right\| \textbf{if} \ \ \left[\!\left[\hat{\underline{U}}\right]\!\right].\underline{n} = 0 \tag{19}$$

Where σ_0 represents the resistance value of the material in traction-compression state.
This criterion is applied to metals and cohesive soils without friction, such as clay soils.

NUMERICAL ANALYSIS

1.5 FAIULURE MECHANISM I

The Prandtl mechanism [13], Fig. 2, has three differentiated zones; zone 1 with a triangular wedge shape with vertical velocity, zone 2 with a logarithmic spiral-shaped rupture surface, and zone three with a displacement with a plane failure surface.

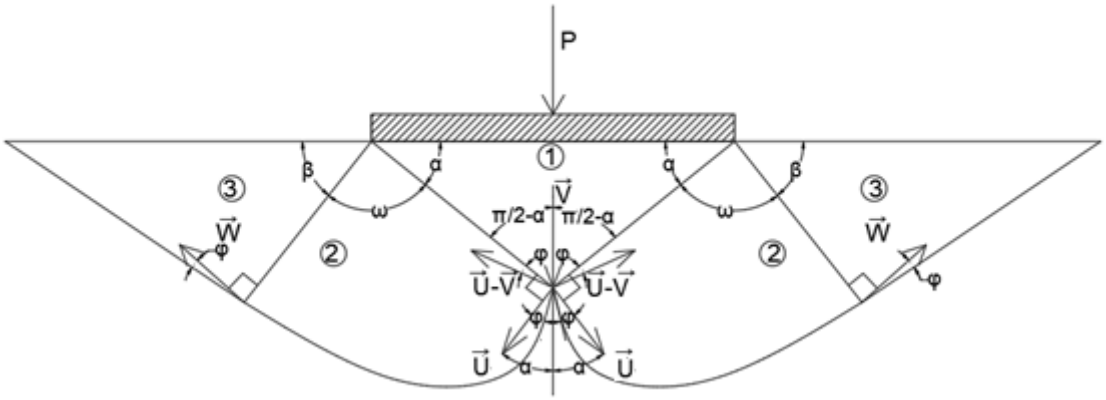

Figure 2. Prandtl's mechanism.

The rate of work P_{ex} performed by external forces is obtained by:

$$P_{ext} = P_{vertical} + P_{1ext} + P_{2ext} + P_{3ext} \tag{20}$$

Where:

$$P_{vertcial} = PV \tag{21}$$

$$P_{1ext} = \frac{\gamma B^2 V}{4}\tan(\alpha) \tag{22}$$

$$P_{2ext} = \frac{1}{2}\gamma\left(\frac{B}{2\cos(\alpha)}\right)^2\left(\frac{V\cos(\alpha-\phi)}{\cos(\phi)}\right)$$
$$\left(\frac{(3\tan(\phi)\cos(\alpha)+\sin(\alpha)+(3\tan(\phi)\cos(\beta)-\sin(\beta))e^{3\omega\tan(\phi)}}{1+9\tan^2(\phi)}\right) \tag{23}$$

$$P_{3ext} = -\gamma\left(\frac{B}{2\cos(\alpha)}\right)^2 e^{3\omega\tan(\phi)}\left(\tan(\beta+\phi)\sin(\beta)+\cos(\beta)\right)\sin(\beta)\frac{V\cos(\alpha-\phi)}{\cos(\phi)}\cos(\beta) \tag{24}$$

Maximum resistive work P_{rm} is obtained through Eq. (4). Using pi functions, Eq. (9), for a Mohr-Columb material, Eq. (11) and Eq. (12):

$$P_{rm} = \underline{Q}.\underline{q}(\hat{\underline{U}}) = \int_{\Omega}\frac{C}{\tan\phi}tr\hat{\underline{\underline{d}}}d\Omega + \int_{\Sigma_{\hat{U}}}\frac{C}{\tan\phi}[[\underline{\hat{U}}]].\underline{n}d\Sigma \tag{25}$$

But $C = 0$, because the soil is granular

$$\therefore P_{rm} = 0 \tag{26}$$

Applying the fundamental kinematic equality:

$$P_{ext} < P_{rm}$$

$$P_{ext} < 0$$

$$P_{vertical} + P_{1ext} + P_{2ext} + P_{3ext} < 0 \tag{27}$$

$$\frac{2P}{\gamma B^2} < 2\left(-\frac{\tan(\alpha)}{4} - \left(\frac{1}{2\cos(\alpha)}\right)^2\left(\frac{\cos(\alpha-\phi)}{\cos(\phi)}\right)\right.$$

$$\times\left(\frac{(3\tan(\phi)\cos(\alpha)+\sin(\alpha)+(3\tan(\phi)\cos(\beta)-\sin(\beta))e^{3\omega\tan(\phi)}}{1+9\tan^2(\phi)}\right)$$

$$\left.+\left(\frac{1}{2\cos(\alpha)}\right)^2 e^{3\omega\tan(\phi)}\left(\tan(\beta+\phi)\sin(\beta)+\cos(\beta)\right)\sin(\beta)\frac{\cos(\alpha-\phi)}{\cos(\phi)}\cos(\beta)\right) \tag{28}$$

With:

$$\phi < \alpha < \frac{\pi}{2}$$

$$\frac{\pi}{2} - \alpha + \phi < \omega < \pi - \alpha$$

$$\beta = \pi - \alpha - \omega \tag{29}$$

1.6 FAILURE MECHANISM II

Hill's mechanism [14] consists of three zones. The first is an irregularly shaped triangular wedge with S velocity, whose vertical component is equal to the velocity of displacement of the footing, the second with a failure mechanism in form of a logarithmic spiral and U velocity, and the third with a plane failure mechanism. See Fig. 3.

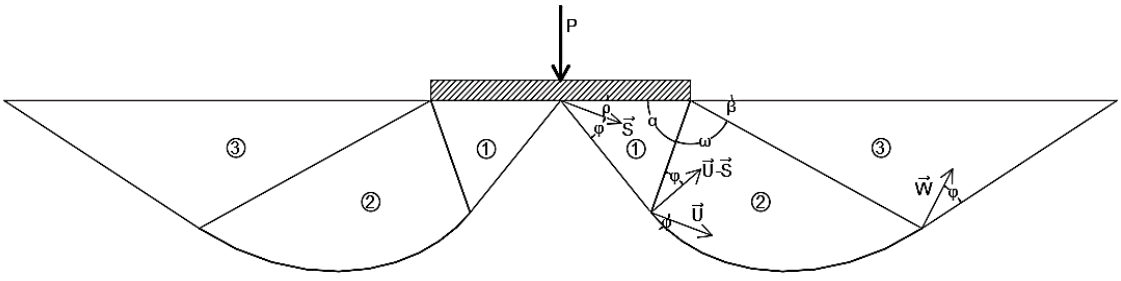

Figure 3. Hill's mechanism.

As the failure mechanism I, P_{ex} is written:

$$P_{ext} = P_{vertical} + P_{1ext} + P_{2ext} + P_{3ext} \tag{30}$$

$$P_{vertical} = PV \tag{31}$$

$$P_{1ext} = \frac{\gamma B}{4}\left(\frac{B\sin(\rho+\phi)}{2\sin(\pi-(\rho+\phi)-\alpha)}\times\sin(\alpha)\right) \tag{32}$$

$$P_{2ext} = \gamma\left(\frac{B\sin(\rho+\phi)}{2\sin(\pi-\rho-\phi-\alpha)}\right)^2\left(\frac{V\sin(\pi+\phi-\alpha-\rho)}{\sin(\rho)\cos(\phi)}\right)$$
$$\times\left(\frac{(3\tan(\phi)\cos(\alpha)+\sin(\alpha)+(3\tan(\phi)\cos(\beta)-\sin(\beta))e^{3\omega\tan(\phi)}}{1+9\tan^2(\phi)}\right) \tag{33}$$

$$P_{3ext} = -\gamma\left(\frac{B\sin(\rho+\phi)}{2\sin(\pi-\rho-\phi-\alpha)}\right)^2 e^{3\omega\tan(\phi)}\left(\tan(\beta+\phi)\sin(\beta)+\cos(\beta)\right)\sin(\beta) \tag{34}$$
$$\times\frac{V\sin(\pi+\phi-\alpha-\rho)}{\sin(\rho)\cos(\phi)}\cos(\beta)$$

Here P_{rm} is null, therefore:

$$P_{ext} < P_{rm}$$

$$P_{ext} < 0$$

$$P_{vertical} + P_{1ext} + P_{2ext} + P_{3ext} < 0 \tag{35}$$

$$\frac{2P}{\gamma B^2} < 2\left(-\frac{\sin(\rho+\phi)\sin(\alpha)}{4\sin(\pi-\rho-\phi-\alpha)} - \left(\frac{\sin(\rho+\phi)}{2\sin(\pi-\rho-\phi-\alpha)}\right)^2\left(\frac{\sin(\pi+\phi-\alpha-\rho)}{\sin(\rho)\cos(\phi)}\right)\right.$$
$$\times\left(\frac{(3\tan(\phi)\cos(\alpha)+\sin(\alpha)+(3\tan(\phi)\cos(\beta)-\sin(\beta))e^{3\omega\tan(\phi)}}{1+9\tan^2(\phi)}\right)$$
$$\left.+\left(\frac{\sin(\rho+\phi)}{2\sin(\pi-\rho-\phi-\alpha)}\right)^2 e^{3\omega\tan(\phi)}\left(\tan(\beta+\phi)\sin(\beta)+\cos(\beta)\right)\sin(\beta)\frac{\sin(\pi+\phi-\alpha-\rho)}{\sin(\rho)\cos(\phi)}\cos(\beta)\right) \tag{36}$$

With:

$$\phi < \alpha < \pi$$

$$\frac{\pi}{2} - \alpha + \phi < \rho < \frac{\pi}{2} - \phi$$

$$\frac{\pi}{2} - \alpha + \phi < \omega < \pi - \alpha$$

$$\beta = \pi - \alpha - \omega \tag{37}$$

1.7 FAILURE MECHANISM III

This is based on the Prandtl mechanism, but with zones 4 and 5 added because of the soil-cement layer. As shown in the Fig. 4, zone 1 has a triangular wedge shape that displaces vertically at the same velocity as the foundation and reinforcement. Region 2 presents a failure mechanism in the form of a logarithmic spiral, where the velocity at the point of contact with region 1 is perpendicular to the discontinuity surface. In region 3 the failure mechanism is a straight plane, where the discontinuity velocity is the same as the final velocity at the point where the failure surface of region 2 and 3 are tangent.

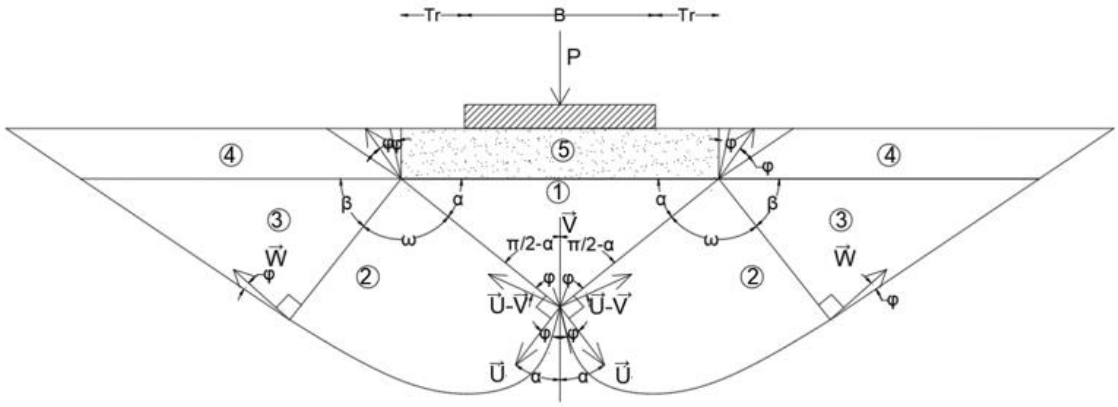

Figure 4. Prandtl's mechanism for a soil reinforced with a soil-cement layer

In this case, the works appear due to the weight 4 and 5.

$$P_{ext} = P_{vertical} + P_{1ext} + P_{2ext} + P_{3ext} + P_{4ext} + P_{5_{ext}} \tag{38}$$

$$P_{vertical} = PV \tag{39}$$

$$P_{1ext} = \frac{\gamma B_r^2 V}{4}\tan(\alpha)$$

$$P_{2ext} = \frac{1}{2}\gamma\left(\frac{B_r}{2\cos(\alpha)}\right)^2\left(\frac{V\cos(\alpha-\phi)}{\cos(\phi)}\right) \tag{40}$$
$$\times\left(\frac{(3\tan(\phi)\cos(\alpha)+\sin(\alpha)+(3\tan(\phi)\cos(\beta)-\sin(\beta))e^{3\omega\tan(\phi)}}{1+9\tan^2(\phi)}\right)$$

$$P_{3ext} = -\gamma\left(\frac{B_r}{2\cos(\alpha)}\right)^2 e^{3\omega\tan(\phi)}\left(\tan(\beta+\phi)\sin(\beta)+\cos(\beta)\right)\sin(\beta)\frac{V\cos(\alpha-\phi)}{\cos(\phi)}\cos(\beta) \tag{41}$$

$$P_{4ext} = -\frac{V\cos(\alpha-\phi)e^{\omega\tan(\phi)}}{\cos(\phi)}\cos(\beta)\times(\gamma\left(\left(\frac{1}{\cos(\alpha)}\right)e^{\omega\tan(\phi)}\cos(\beta)+\tan(\beta+\phi)\left(\frac{1}{\cos(\alpha)}\right)e^{\omega\tan(\phi)}\sin(\beta)\right)$$
$$\times\frac{B_r^2 n}{1+2mn}+\gamma\left(\tan(\beta+\phi)-\tan(\beta-\phi)\right)\frac{B_r^2 n^2}{(1+2mn)^2}) \tag{42}$$

$$P_{5ext} = \frac{\gamma n B_r^2 V}{(1+2nm)} \tag{43}$$

Using the kinematics approach:

$$P_{ext} < P_{rm}$$
$$P_{ext} < 0$$
$$P_{vertical} + P_{1ext} + P_{2ext} + P_{3ext} + P_{4ext} + P_{5_{ext}} < 0 \tag{44}$$

Resulting:

$$\frac{2P}{\gamma B} < 2(1+2mn)^2\left(-\frac{\sin(\rho+\phi)\sin(\alpha)\gamma}{4\sin(\pi-\rho-\phi-\alpha)} - \gamma\left(\frac{\sin(\rho+\phi)}{2\sin(\pi-\rho-\phi-\alpha)}\right)^2\left(\frac{\sin(\pi+\phi-\alpha-\rho)}{\sin(\rho)\cos(\phi)}\right)\right.$$
$$\times\left(\frac{(3\tan(\phi)\cos(\alpha)+\sin(\alpha)+(3\tan(\phi)\cos(\beta)-\sin(\beta))e^{3\omega\tan(\phi)}}{1+9\tan^2(\phi)}\right)$$
$$+\gamma\left(\frac{\sin(\rho+\phi)}{2\sin(\pi-\rho-\phi-\alpha)}\right)^2 e^{3\omega\tan(\phi)}\left(\tan(\beta+\phi)\sin(\beta)+\cos(\beta)\right)\sin(\beta)\frac{\sin(\pi+\phi-\alpha-\rho)}{\sin(\rho)\cos(\phi)}\cos(\beta)$$
$$+\frac{\cos(\alpha-\phi)e^{\omega\tan(\phi)}}{\cos(\phi)}\cos(\beta)\times\left(\gamma\left(\left(\frac{1}{\cos(\alpha)}\right)e^{\omega\tan(\phi)}\cos(\beta)+\tan(\beta+\phi)\left(\frac{1}{\cos(\alpha)}\right)e^{\omega\tan(\phi)}\sin(\beta)\right)\frac{n}{1+2mn}\right.$$
$$\left.\left.+\gamma\left(\tan(\beta+\phi)-\tan(\beta-\phi)\right)\frac{n^2}{(1+2mn)^2}\right)-\frac{n}{(1+2nm)}\right) \tag{45}$$

With:

$$\phi<\alpha<\frac{\pi}{2}$$
$$\frac{\pi}{2}-\alpha+\phi<\omega<\pi-\alpha$$
$$\beta=\pi-\alpha-\omega \tag{46}$$

1.8 FAILURE MECHANISM IV

Starting from the Hill's mechanism, zones 4 and 5 are added, as illustrated in Fig. 5. Zone 4 moves vertically with the foundation speed, while zone 5 has the same speed as zone 3.

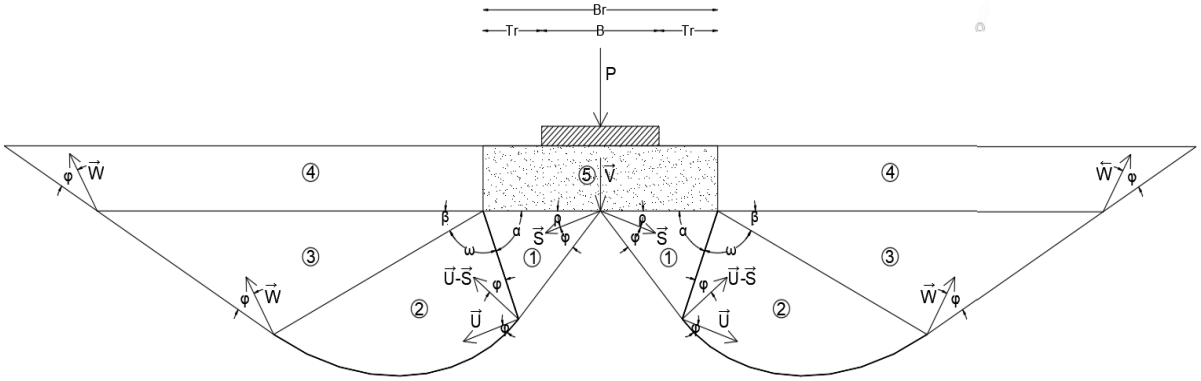

Figure 5. Hill's mechanism for a soil reinforced with a soil-cement layer

For this mechanism:

$$P_{ext} = P_{carga\_vertical} + P_{1ext} + P_{2ext} + P_{3ext} + P_{4ext} + P_{5_{ext}} \tag{47}$$

And:

$$P_{vertical} = PV \tag{48}$$

$$P_{1ext} = \frac{B_r^2\sin(\rho+\phi)\sin(\alpha)V\gamma}{4\sin(\pi-\rho-\phi-\alpha)} \tag{49}$$

$$P_{2ext} = \gamma\left(\frac{B_r\sin(\rho+\phi)}{2\sin(\pi-\rho-\phi-\alpha)}\right)^2\left(\frac{V\sin(\pi+\phi-\alpha-\rho)}{\sin(\rho)\cos(\phi)}\right)$$
$$\times\left(\frac{(3\tan(\phi)\cos(\alpha)+\sin(\alpha)+(3\tan(\phi)\cos(\beta)-\sin(\beta))e^{3\omega\tan(\phi)}}{1+9\tan^2(\phi)}\right) \tag{50}$$

$$P_{3ext} = -\gamma\left(\frac{B_r \sin(\rho+\phi)}{2\sin(\pi-\rho-\phi-\alpha)}\right)^2 e^{3\omega\tan(\phi)}\left(\tan(\beta+\phi)\sin(\beta)+\cos(\beta)\right)\sin(\beta) \times\frac{V\sin(\pi+\phi-\alpha-\rho)}{\sin(\rho)\cos(\phi)}\cos(\beta) \tag{51}$$

$$P_{4ext} = -\left(\frac{V\sin(\pi+\phi-\alpha-\rho)}{\sin(\rho)\cos(\phi)}\right)e^{\omega\tan(\phi)}\cos(\beta)\times(\gamma\left(\left(\frac{1}{\cos(\alpha)}\right)e^{\omega\tan(\phi)}\cos(\beta)+\tan(\beta+\phi)\left(\frac{1}{\cos(\alpha)}\right)e^{\omega\tan(\phi)}\sin(\beta)\right) \times\frac{B_r^2 n}{1+2mn}+\gamma\left(\tan(\beta+\phi)-\tan(\beta-\phi)\right)\frac{B_r^2 n^2}{(1+2mn)^2}) \tag{52}$$

$$P_{5ext} = \frac{\gamma n B_r^2 V}{(1+2nm)} \tag{53}$$

In a similar way to the previous cases, applying the yield design:

$$\frac{2P}{\gamma B^2} < 2(1+2mn)^2(-\frac{\sin(\rho+\phi)\sin(\alpha)}{4\sin(\pi-\rho-\phi-\alpha)}-\left(\frac{\sin(\rho+\phi)}{2\sin(\pi-\rho-\phi-\alpha)}\right)^2 \times\left(\frac{\sin(\pi+\phi-\alpha-\rho)}{\sin(\rho)\cos(\phi)}\right)\times\left(\frac{(3\tan(\phi)\cos(\alpha)+\sin(\alpha)+(3\tan(\phi)\cos(\beta)-\sin(\beta))e^{3\omega\tan(\phi)}}{1+9\tan^2(\phi)}\right) +\left(\frac{\sin(\rho+\phi)}{2\sin(\pi-\rho-\phi-\alpha)}\right)^2 e^{3\omega\tan(\phi)}\left(\tan(\beta+\phi)\sin(\beta)+\cos(\beta)\right) \times\sin(\beta)\frac{\sin(\pi+\phi-\alpha-\rho)}{\sin(\rho)\cos(\phi)}\cos(\beta)+W\cos(\beta) \times(\left(\left(\frac{\sin(\rho+\phi)}{\sin(\pi-\rho-\phi-\alpha)}\right)e^{\omega\tan(\phi)}\cos(\beta)+\tan(\beta+\phi)\left(\frac{\sin(\rho+\phi)}{\sin(\pi-\rho-\phi-\alpha)}\right)e^{\omega\tan(\phi)}\sin(\beta)\right) \times\frac{n}{1+2mn}+\left(\tan(\beta+\phi)-\tan(\beta-\phi)\right)\frac{n^2}{(1+2mn)^2})-\frac{n}{1+2mn}) \tag{54}$$

With:

$$\begin{aligned}&\phi<\alpha<\pi\\&\frac{\pi}{2}-\alpha+\phi<\rho<\frac{\pi}{2}-\phi\\&\frac{\pi}{2}-\alpha+\phi<\omega<\pi-\alpha-\phi\\&\beta=\pi-\alpha-\omega\end{aligned} \tag{55}$$

RESULTS

The numerical analysis software Scilab [15] is used to determinate the results. The values obtained are compared in Table 2 with those determined by: Kumbhojkar [16], Terzaghi load capacity theory [17]; Chen using limit analysis for the solution of the Prandtl and Hill mechanism; Meyerhof considering the limit equilibrium theory [18]; and Foppa's tests using reduced models.

The results are expressed as a function of the factor N_γ.

Table 2. Factor N_γ for various studies for unreinforced soils.

Method	$\phi = 10°$	$\phi = 15°$	$\phi = 20°$	$\phi = 25°$	$\phi = 35°$	$\phi = 40°$
Faiulure mechanism I	2.72	5.88	12.42	26.8	60.32	146.8
Faiulure mechanism II	1.16	2.62	5.7	12.5	28.62	70.28
Kumbhojkar (from Terzaghi)	1.52	3.64	8.34	19.14	45.52	115.3
Chen (from Prandtl)	2.74	5.88	12.4	26.7	60.2	147
Chen (from Hill)	1.16	2.68	5.9	12.7	28.6	71.6
Meyerhof	2.5	5.5	12	26	60	130
Foppa	-	-	-	-	60.75	-

The results obtained for the soil reinforced with the soil-cement layer are compared in Table 3 with the results of Foppa, for an internal friction angle of 35°, by varying the parameters $\frac{H_r}{B}$ and $\frac{T_r}{H_r}$.

Table 3. Factor N_γ for foundations reinforced with soil-cement ($\phi = 35°$).

$\frac{H_r}{B}$	$\frac{T_r}{H_r}$	N_γ *Foppa*	N_γ *Yield design*	*Error (%)*
0.25	0.25	71.3	60.2	18.3
0.25	0.50	70.7	70.7	0.0
0.25	1.00	111.0	96.5	14.9
0.50	0.25	93.6	72.5	5.3
0.50	0.25	82,8	98.9	16.2
0.50	0.25	82.6	99.4	16.4

The mechanism with lower N_γ values is failure mechanism III for small ϕ, and failure mechanism IV for large ϕ. Therefore, according to the kinematic approach, the failure mechanism depends on the ϕ angle of the soil. Comparing these results with the results of the reduced model, it is obtained that the greatest error present is of 18,3% that is presented in the case of $n = 0,25$ and $m = 0,25$.

The values of the load capacity N_γ are expressed as a function of the parameters $m = \frac{H_r}{B}$, $n = \frac{T_r}{H_r}$, through the curves shown in Fig. 6, Fig. 7 and Fig. 8. Defining m and n, with an input value ϕ, it is obtained the value of N_γ. These graphs were made based on the failure mechanism that gives the lowest load capacity for each particular ϕ, m and n., because this was the one that gave a lower load capacity. It is important to clarify that this analysis does not include the possibility of the failure of the soil-cement layer. It is necessary to verify that the failure of the soil-cement layer will not occur before. If this effect is to be considered, it is advisable to perform indirect tensile tests to determine the maximum flection moment that the soil-cement layer can support. The instant when is produced the reinforcement failure is under analysis yet.

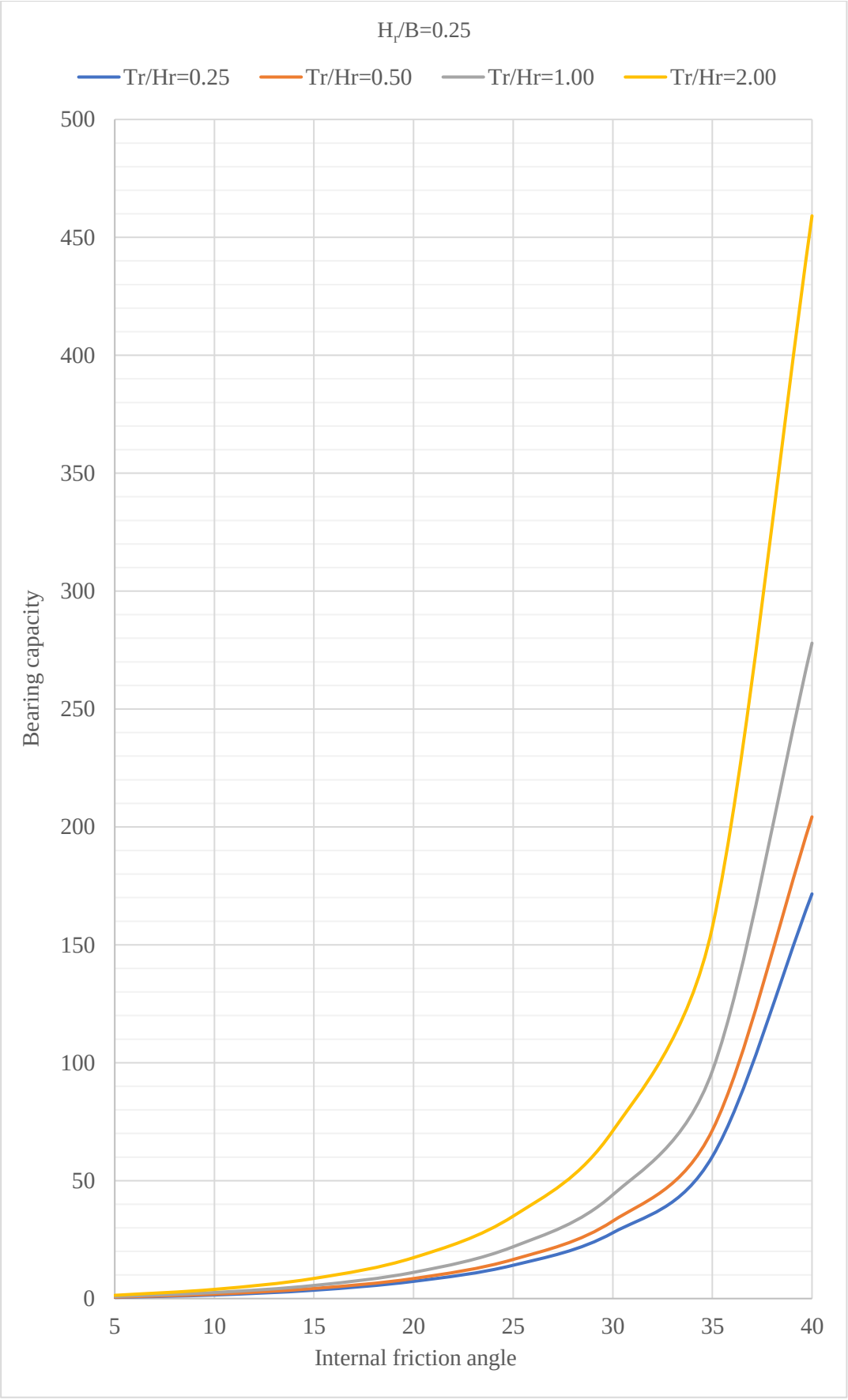

Figure 6. Curve N_γ - ϕ for $m = \frac{H_r}{B} = 0.25$.

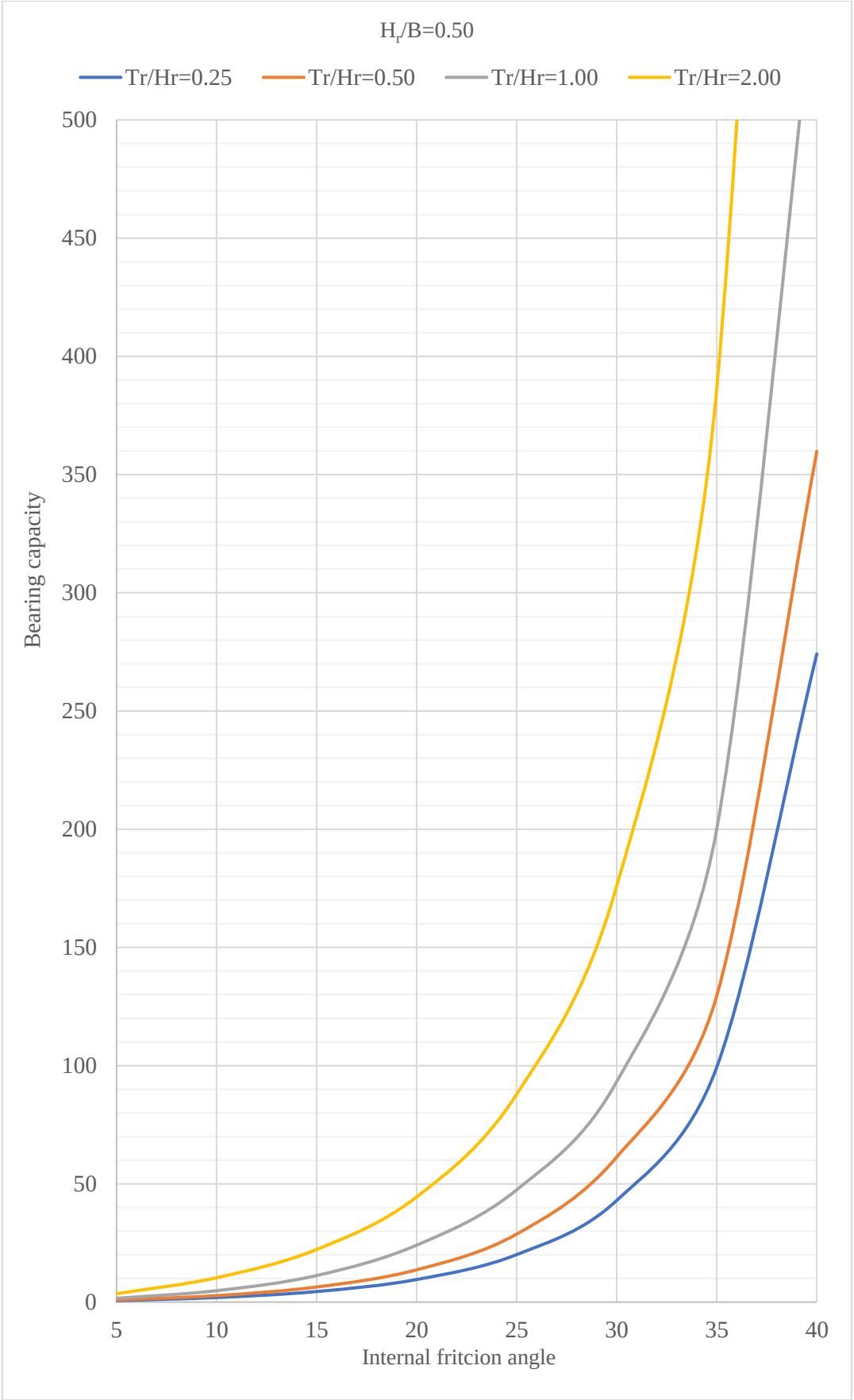

Figure 7. Curve N_γ - ϕ for $m = \frac{H_r}{B} = 0.50$.

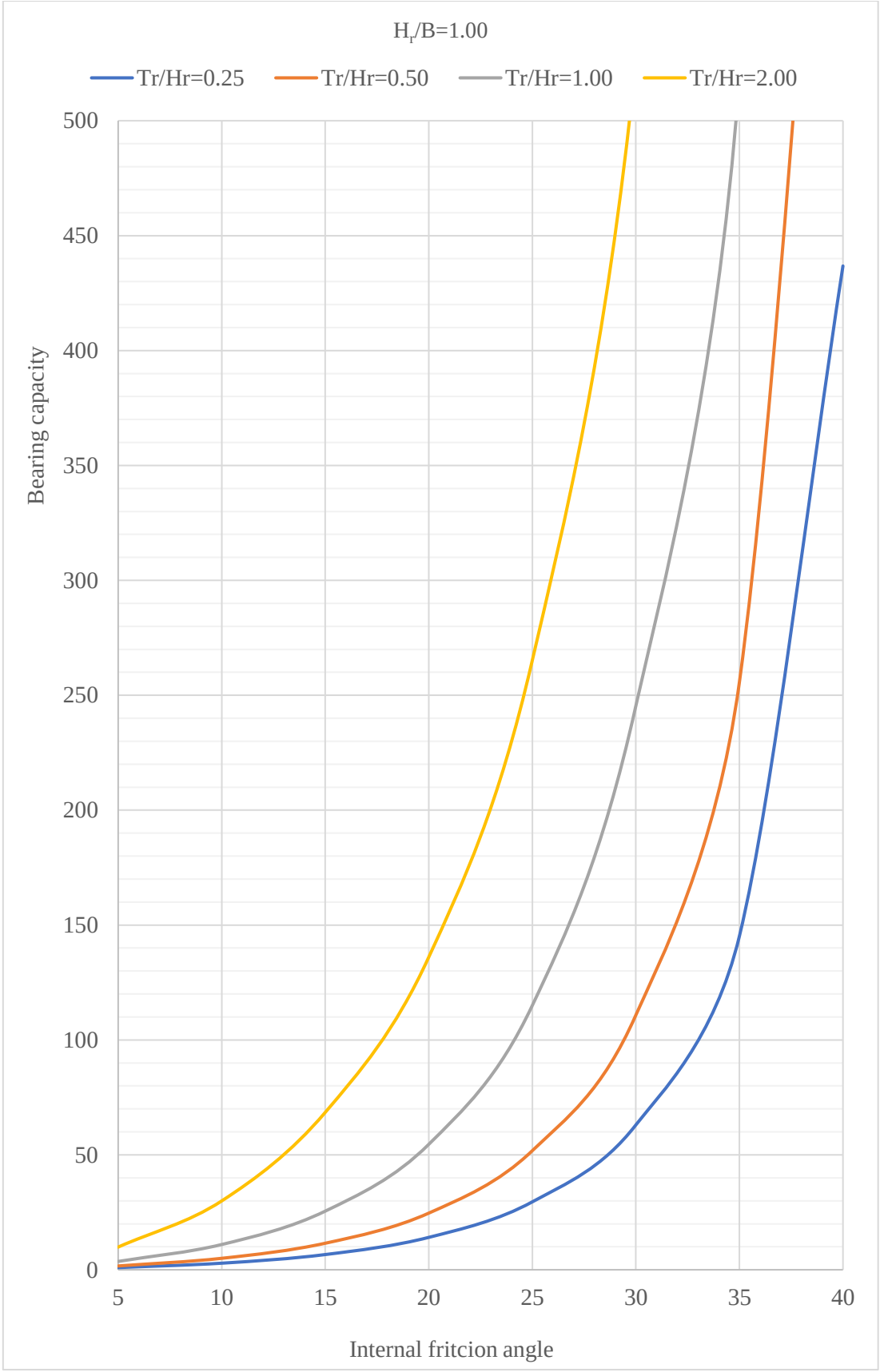

Figure 8. Curve N_γ - ϕ for $m = \frac{H_r}{B} = 1.00$.

CONCLUSIONS

First of all, it is clearly appreciable that there is an increase in the load capacity vertically distributed on the z-axis in shallow foundations reinforced with a layer of soil-cement. For the analysis the Prandtl and Hill failure mechanisms were used with the dynamic approach of yield design. The results of this investigation are compared with those obtained by other authors.

The novelty of this work is that analytical results of the load capacity forecast are presented from abacus, which are obtained from dimensional formulas that due to their complexity were tabulated by using the numerical analysis software Scilab.

It must be taken into account that the failure of the reinforcement is not considered, so for considerable dimensions of the reinforcement in relation to the width of the footing, the results obtained may be oversized. The determination of the load under which the reinforcement fails is still being studied.

REFERENCES

[1] R. L. Sacco, «Metodologia de Projeto de Fundações Superficiais Assentes sobre Camada de Reforço em Solo-Cimento», 2016.

[2] J. G. Rossi, «Fundações circulares apoiadas em camadas de solo-cimento de área variável implantadas em solo coesivo-friccional de baixa capacidade de suporte», p. 144.

[3] M. Forcelini, G. R. Garbin, V. P. Faro, y N. C. Consoli, «Mechanical behavior of soil cement blends with Osorio sand», *Procedia engineering*, vol. 143, pp. 75-81, 2016.

[4] I. E. de la Fuente Lavalle y Instituto Mexicano del Cemento y del Concreto, *Suelo-Cemento: sus usos, propiedades y aplicaciones*. México: Instituto Mexicano del Cemento y del Concreto, 1995.

[5] J. T. Corral, «El suelo-cemento como material de construcción (Ground-Cement as a construction material)», *Ciencia y Sociedad*, p. 53, 2008.

[6] M. A. Vendruscolo, «Análise numérica e experimental do comportamento de fundações superficiais assentes em solo melhorado», 1996.

[7] D. Foppa, «Novo método para cálculo da capacidade de carga de fundações superficiais assentes sobre camada de reforço em solo cimento», 2016.

[8] R. L. Corrêa, L. A. Bressani, F. B. Martins, y D. de, «Influência da densidade na resistência à compressão simples de um solo», p. 1.

[9] G. W. Clough, N. Sitar, R. C. Bachus, y N. S. Rad, «Cemented sands under static loading», *Journal of Geotechnical and Geoenvironmental Engineering*, vol. 107, n.º GT6, jun. 1981.

[10] O. G. Ingles y J. B. Metcalf, «Soil stabilization principles and practice», 1972.

[11] J. Salençon, *Yield design*. Hoboken, N.J.: ISTE Ltd/John Wiley and Sons Inc, 2013.

[12] W.-F. Chen, *Limit analysis and soil plasticity*. Amsterdam ; New York: Elsevier Scientific Pub. Co, 1975.

[13] L. Prandtl, «Über die Härte plastischer Körper», *Nachrichten von der Gesellschaft der Wissenschaften zu Göttingen, Mathematisch-Physikalische Klasse*, vol. 1920, pp. 74-85, 1920.

[14] R. Hill, «The mathematical theory of plasticity, Clarendon», *Oxford*, vol. 613, p. 614, 1950.

[15] S. Enterprises, «Scilab: Free and Open Source software for numerical computation», *Scilab Enterprises, Orsay, France*, vol. 3, 2012.

[16] A. S. Kumbhojkar, «Numerical evaluation of Terzaghi's N γ», *Journal of Geotechnical Engineering*, vol. 119, n.º 3, pp. 598–607, 1993.

[17] K. Terzaghi, «Theoretical soil mechanics, Wiley, New York», 1943.

[18] G. G. Meyerhof, «The ultimate bearing capacity of foudations», *Geotechnique*, vol. 2, n.º 4, pp. 301–332, 1951.